Ultrasound Tissue Characterization of the Normal Kidney

Ana Luiza D. Valiente Engelhorn, MD, MS,† Carlos Alberto Engelhorn, MD, PhD,*† Sergio X. Salles-Cunha, PhD, RVT, FSVU,* Ricardo Ehlert,† Fernando Kenji Akiyoshi,† and Kassyana Weinfurter Assad†*

Aim: Ultrasound tissue characterization (USTC) is a precursor of ultrasound virtual histology (USVH), already applied to B-mode images of coronary, carotid, and peripheral arteries, as well as venous thrombosis. Elevated echogenicity has been described for a rejected transplanted kidney. We analyzed data from healthy young adults as reference for further renal USTC.

Methods: Ultrasound kidney images of 10 volunteers were analyzed. Pixel brightness in the 0-to-255 range was rescaled to zero for black and 200 for fascia brightness before automatic classification into 14 ranges, including "blood-like" (0–4), "fat-like" (8–26), "hypoechoic muscle-like" (41–60), "hyperechoic muscle-like" (61–76), 4 ranges of "fiber-like" (112–196), "calcium-like" (211–255) and intermediary intervals. Nomenclature was readapted using nonechoic, hypoechoic I to IV, echoic I to IV, hyperechoic I to IV, and saturated echoes to avoid inference to actual kidney tissue. Descriptive and comparative statistics were based on percentages of pixels in specific brightness ranges.

Sample Population: Eight women and 2 men, 26 ± 4 years (range, 22–34 years) old, were studied. Kidney length was 10.5 ± 0.9 cm (9.0–12.0 cm). Doppler US resistivity index was 0.67 ± 0.03 (0.62–0.71).

Results: Original fascia brightness converted to 200 value had a mean ± SD of 206 ± 16 (range, 181–236). Kidney grayscale median averaged 37 ± 6 (27–48). Most pixels were hypoechoic II to IV (8–60), averaging 78% ± 6% (66%–87%). Percentages for fat-like, intermediary fat/muscle-like, and hypoechoic muscle-like intervals averaged 25%, 28%, and 25%, respectively.

Conclusions: A reference database for USTC/USVH of normal young kidneys was created for future comparisons with transplanted and abnormal kidneys. Normal renal echoes have low brightness. Hyperechoic pixels may represent abnormalities.

Key Words: kidney, ultrasound imaging, B-mode ultrasound, computer-assisted image processing, virtual histology, grayscale median; GSM

(*Ultrasound Quarterly* 2012;28:275–280)

Ultrasound virtual histology (USVH) allows for quantification and tissue characterization (USTC) based on the brightness of echoes forming a B-mode image. Extensive literature describes correlations between intravascular ultrasound (IVUS) and histological findings of coronary and carotid atheromas.[1,2] Transcutaneous USVH has been applied to the carotid artery; echo brightness ranges were associated to fat, muscle, fiber, and calcium.[3]

Calculation of the grayscale median, or GSM, is a practical, quantitative simplification. Carotid plaques with low GSM have been linked to a high incidence of cerebrovascular symptoms during stenting.[4] The GSM of peripheral femoral atherosclerosis may predict ease of reentry during intimal dissection treatment.[5] Grayscale median increases as deep venous thrombosis progresses from acute to subacute.[6] Presently, we are involved in USTC research related to B-mode images of carotid arteries,[7] venous thrombosis,[8] peripheral arterial obstruction, different types of leg edema,[9] and organ tissue analysis. A case related to transplanted kidney rejection has been presented.[10] Ultrasound tissue characterization demonstrated a trend toward abnormally increased echogenicity before symptoms appeared or renal resistivity index (RI) increased. Furthermore, several kidneys of symptomatic patients examined in our laboratory appeared to have abnormally hyperechoic regions.

This investigation is an initial step on the validation of renal USTC as a precursor protocol for USVH. Data from healthy young adults have been collected for future reference during studies of transplanted kidneys and several renal abnormalities. The analysis was performed on postprocessed output images provided by a standard high-definition ultrasound instrument. Noise reduction, for example, is one reason for postprocessing commonly used by manufacturers. Tissue characterization analysis may be dependent on instrumentation design and its image processing requirements. Nevertheless, our approach was practical and applicable to images obtainable in clinical practice.

MATERIALS AND METHODS

Volunteers had their kidneys imaged at an International Standard Organization-accredited noninvasive vascular laboratory, Angiolab-Curitiba, of a major city south of Brazil. This project was part of protocol number 5782 approved by the Ethics Research Committee of Pontificia Universidade Católica do Paraná.

This session describes basics of the ultrasound imaging procedure and summarizes the USTC technique. Basic statistics used are also mentioned.

Ultrasonography

Standard US imaging was performed by a physician with 20 years' experience at an International Standard Organization-certified vascular laboratory.[11] Subjects were examined in lateral

Received for publication May 3, 2012; accepted July 29, 2012.

*Angiolab, Inc, Noninvasive Vascular Laboratory, Curitiba, PR, Brazil; and †Pontificia Universidade Católica do Paraná Curitiba, PR, Brazil.

The authors declare no conflict of interest.

Reprints: Sergio Xavier Salles-Cunha, PhD, RVT, FSVU and Carlos Alberto Engelhorn, MD, PhD, Angiolab Curitiba, Inc, Rua da Paz, 195, sala 2, Alto da XV, Curitiba, PR, Brazil CEP 80060-160 (Angiolab) or Rua José Casagrande, 1310, Vista Alegre, Curitiba CEP 80820-590, PR, Brazil (e-mail: sallescunha@yahoo.com; carlos.engelhorn@pucpr.br).

decubitus. A Siemens-Acuson (Issaquah, WA) Antares scanner and a curved-array 2–6 MHz probe were used. Images used for USTC were optimized for measurement of kidney size or length. Standard instrument preset determined the grayscale mapping used. The basic protocol recommended minimal or no alterations in time gain control or any other knob adjustment. Minimal adjustments were made, if necessary, to maintain the white "fascia-like" regions similar in echogenicity throughout the kidney tissue. Improving human visual perception of the image was not part of the protocol. Minimal or no changes from standard preset were followed by one physician only to minimize setting and interobserver variability. Kidney length and resistivity indices (RIs) based on the ratio between systolic and diastolic velocities measured in intrarenal interlobar, arcuate, and cortical arteries were calculated and described in the sample population session of results. Color Doppler confirmed normalcy of kidney perfusion and minimized kidney scanning and number of IR determinations. Changes in instrument settings were minimized to depth and focus selection. Image improvements based on human eye visualization were avoided.

Image Analysis

Pixel brightness analysis of the recorded image (in our case, recorded as jpeg) can be performed with photography programs commercially available.[5] We opted for an in-house program, validated on numerous applications, designed to provide flexibility in the GSM calculation and selection of brightness intervals and colors.[6–10,12]

USTC

Each kidney image was submitted to USTC 3 times. The second and third analyses for each kidney were used only to confirm the findings of the first analysis and did not enter in the statistical evaluation. Two of 60 USTC analyses were rejected as having technical errors or inconsistencies. Otherwise, maximum and minimum GSM measured for the same kidney did not vary by more than 20%, calculated as their difference divided by their mean. Therefore, 18 and 2 kidneys had similar results 3 and 2 times, respectively.

Carotid plaque pixel characterization by Lal et al[3] was adapted to kidney analysis.

Pixel brightness was rescaled to improve uniformity among images and to become less dependent on individual tissue attenuation. A black region of the image represented zero. The USTC analyst selected manually a bright fascia to represent the 200 level of a 0-to-255 image range. Intervals of pixel brightness for blood-like, fat-like, and calcium-like were kept the same as that of Lal et al.[3] Muscle brightness interval was subdivided into hypoechoic and hyperechoic muscle-like intervals. Fiber brightness interval was subdivided into 4 intervals: hypo, mid-hypo, mid-hyper, and hyperechoic fiber-like intervals. Default brightness interval ranges were specifically identified. These intervals included the blood-fat, fat-hypoechoic muscle, hyperechoic muscle-fiber and fiber-calcium ranges. Percentages of pixel brightness were calculated for each of the 14 intervals. Some intervals were grouped in the analysis as a function of results.

A general description of tissue characterization for the brightness intervals was selected to avoid direct virtual histology connotation to fat, muscle, fiber, and calcium. The intervals in the 0-to-255 echo brightness range were named: nonechoic (0–4); hypoechoic I (5–7), II (8–26), III (27–40), and IV (41–60); echoic I (61–76), II (77–90), III (91–110), and IV (112–132); hyperechoic I (133–153), II (154–174), III (175–196), and IV(197–210); and saturated (211–255). Figure 1 shows an example.

Statistics

Grayscale median was calculated and analyzed specifically. Percentage data were interpreted as a continuous variable. Mean, standard deviation, and minimum and maximum values were calculated based on Excel descriptive statistics. A coefficient of variability (CV) was estimated as the ratio deviation/mean. Comparisons between right and left kidneys were based on Student *t* tests, also available with the Excel program.

RESULTS

This session summarizes the sample population studied and provides data related to the USTC scale selection, GSM, and percentages of pixels in each brightness interval.

Sample Population

Ultrasound images of the right and left kidneys were recorded from 10 healthy young volunteers on a first-come, sequential order. Eight volunteers were women and two were men. The mean ± SD age was 26 ± 4, ranging from 22 to 34 years. The mean ± SD kidney length was 10.6 ± 1.0 cm, ranging from 9.0 to 12.0 cm on the right and 10.3 ± 0.8 cm, ranging from 9.3 to 11.3 cm on the left ($P = 0.18$ by paired *t* test). The kidney length was longer in 5 right and 4 left kidneys and equal in 1 kidney. The right was 1.5 cm longer than the left kidney in one subject. Otherwise, absolute differences were 8 mm or less. Resistivity index, based on renal Doppler waveforms, correlated with asymptomatic history, with mean ± SD of 0.67 ± 0.03 bilaterally, ranging from 0.62 to 0.71. Six right kidneys had greater RI, but the absolute difference between right and left RI was 0.07 or less ($P = 0.75$ by paired *t* test).

USTC Scale

The mean ± SD original brightness of the fascia selected as the 200-point reference was 206 ± 16, ranging from 181 to 236 according to the digital scale of the instrument. The coefficient of variability, CV = SD / mean, was 7.7%. There was no statistically significant difference between these values obtained for the right versus left kidneys: 208 ± 18 versus 203 ± 14 ($P = 0.39$ by paired *t* test).

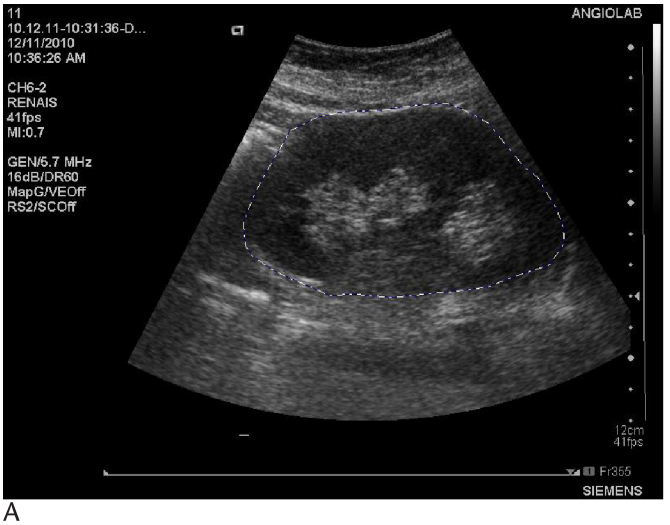

A

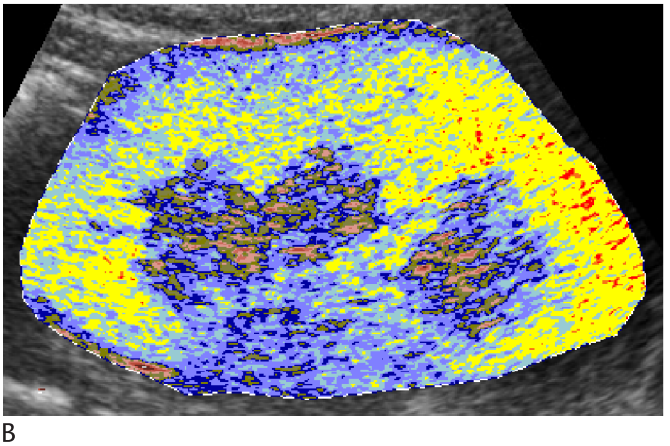

B

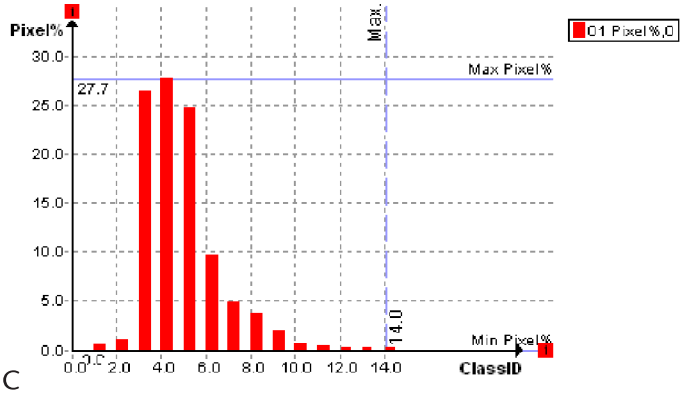

C

Interval Identification (ID)	Grey from	To	Pixel No%	Color
Nonechoic (blood-like)	0	4	0.427	
Hypoechoic I (blood/fat-like)	5	7	0.890	
Hypoechoic II (fat-like)	8	26	26.231	
Hypoechoic III (fat/muscle-like)	27	40	27.664	
Hypoechoic IV (hypoechoic muscle-like)	41	60	24.411	
Echoic I (hyperechoic muscle-like)	61	76	9.580	
Echoic II (hypoechoic muscle/fiber-like)	77	90	4.711	
Echoic III (hyperechoid muscle/fiber-like)	91	111	3.536	
Echoic IV (fiber-like lower level)	112	132	1.771	
Hyperechoic I (fiber-like mid lower lever)	133	153	0.549	
Hyperechoic II (fiber-like midhigher level)	154	174	0.174	
Hyperechoic III (fiber-like mid higher level)	175	196	0.043	
Hyperechoic IV (fiber/calcium-like)	197	210	0.012	
Saturated (white calcium-like)	211	255	0.003	

ID associated with virtual histology of carotid plaques (reference 3); gray scale brightness level from-to based on 256 amplitude levels; percentage of pixels in the interval; color arbitrarily assigned by analyst.

D

FIGURE 1. Example of virtual USTC applied to a normal young kidney. A, B-mode image from a common ultrasound instrument. B, Colorized image representing various pixel brightness levels. C, Histogram showing pixel brightness distribution. D, Table defining 14 levels of grayscale pixel brightness transformed into artificial colors.

GSM

The mean ± SD GSM was 37 ± 6, ranging from 27 to 48, and resulting in a CV equal to 16%. There was no statistically significant difference between these values obtained for the right versus left kidneys: 38 ± 7 versus 37 ± 6 ($P = 0.53$ by paired t test).

USTC Interval Percentages

Table 1 shows the mean, standard deviation, and minimum and maximum values for percentage of pixels in each interval. There was no significant statistical difference between right and left kidneys in the comparisons of percentages in each interval ($0.17 < P < 0.97$). Extremely hypoechoic pixels in the 0-to-7 range were rare and averaged 2.1% of the pixels in the kidney image. On the high brightness side, hyperechoic or saturated pixels averaged 1.1%. Echoic II to IV pixels averaged 9.5%. Therefore, most pixels were in the 8-to-76 range, averaging 87.5% of the pixels.

Most pixels were in the hypoechoic II to IV brightness intervals, with a mean ± SD of 78 ± 6, ranging from 66% to 87% in each kidney. These were the only intervals with percentages greater than 10%. The CV was the lowest for the hypoechoic III interval, 17%, followed by hypoechoic IV and II intervals with CV equal to 21% and 38%, respectively. The CV, however, dropped to 8% when these 3 hypoechoic II to IV groups were combined into one major group.

DISCUSSION

Visual analysis of ultrasound B-mode images is a daily occurrence. Ultrasound tissue characterization represents additional efforts to emphasize image details or to quantify the pixel brightness data. This investigation initiated validation of USTC, or even USVH, applied to the kidney. A case of renal transplant rejection called attention to the fact that the GSM of the transplanted kidney was high, at 60, on day 1 after transplant. This GSM value was higher than all GSM of normal young kidneys included in this study. The percentage of pixels in the range greater than 77 was 33% compared to normal expectancy of less than 11%. Furthermore, the fiber-like pixels were 10% compared to an expected normal 3% of all pixels. These findings

TABLE 1. Ultrasound Tissue Characterization of the Normal Kidney: Descriptive Statistics

Grayscale Brightness			Percentage of Image Pixels (%)	
Identification	Interval	Mean	SD	Min-Max
Nonechoic	0–4	0.9	1.3	0.0–4.4
Hypoechoic I	5–7	1.2	1.2	0.0–3.9
Hypoechoic II	8–26	25.3	9.6	8.2–46.5
Hypoechoic III	27–40	28.1	4.7	19.9–36.0
Hypoechoic IV	41–60	24.6	5.2	15.5–34.3
Echoic I	61–76	9.5	2.6	5.5–14.9
Echoic II	77–90	4.4	1.4	1.9–7.6
Echoic III	91–111	3.4	1.4	1.5–6.8
Echoic IV	112–132	1.7	0.9	0.3–3.4
Hyperechoic I	133–153	0.7	0.5	0.2–2.2
Hyperechoic II	154–174	0.3	0.3	0.0–1.0
Hyperechoic III	175–196	0.1	0.1	0.0–0.3
Hyperechoic IV	197–210	0.02	0.01	0.00–0.04
Saturated	211–255	0.01	0.02	0.00–0.07

Min-Max, minimum-maximum values in the interval.

preceded symptoms and abnormal RIs registered on day 7. We also observed that 31 symptomatic patients referred to our vascular laboratory had abnormally hyperechoic transplanted kidneys, with GSM in the 51-to-83 range. At least half had elevated flow RIs. Confounding factors include characteristics of kidneys from cadaver and live donors. These findings generated an ongoing investigation on the relationship between kidney echogenicity and pathology. Figure 2 shows USTC of a transplanted kidney with a GSM equal to 83 and an IR of 0.77.

Our objective originated from IVUS studies but has a different, practical sense: to improve perception and quantification of transcutaneous, noninvasive, B-mode ultrasound images. Transcutaneous imaging has to correct for variable attenuation more so than IVUS. Intravascular ultrasound has been correlated to histology, and studies have focused on fat, soft tissue/fibrosis, and calcium. Ex vivo histology, however, may not represent in vivo conditions to its fullest. We, therefore, prefer to mention this transcutaneous application as tissue characterization rather than virtual histology.

We now have created a solid database for comparison of USTC examinations of kidneys. Extremely low or high echogenicity, localized or generalized, should raise suspicions of abnormality.

Classical atherosclerotic USVH analysis selects a region of the arterial adventitia for a 190 level of the scale.[3] The value 190 was replaced by an easier-to-remember 200 number. Technically, selection of a fascia reference for scale standardization presented low variability of less than 10% and substituted well for the adventitia. Although this investigation could be considered a learning experience of the kidney, the analyst had used USTC for other applications previously. Only 2 image analyses of the original 60 had unacceptable findings.

We opted for a practical approach applicable to virtually any ultrasound instrument in any laboratory. Perfectionists will point out that the presence of noise and several data processing steps alter the actual signals received at the transducer level. It is possible that original radiofrequency signals must be processed to form practical, clinical images. Ultrasound instruments have to process the signal received to optimize imaging by noise reduction and signal composition. Postprocessing is not the same for all instruments. The common adage is that each laboratory should validate ultrasound findings in-house. This philosophy is valid for flow velocity as well as for B-mode measurements. However, while we wait for technology to reach an optimum stage for USTC, we can apply this practical approach to everyday practice. Furthermore, the more data we collect justifying renal USTC, the higher the likelihood that developers will optimize the electronic technology for USTC or even USVH.

At present, the best application of the kidney or other tissue USTC technology is in the quantitative comparison of data from US images obtained sequentially or longitudinally in the same anatomic region, with the same equipment and settings, and perhaps the same ultrasonographer. We have demonstrated changes not only in a transplanted kidney[10] but also in the evaluation of lymphedema postmassage therapy,[12] and carotid plaque pre endarterectomy versus after endarterectomy (unpublished, not presented yet). Populational studies have demonstrated fat-muscle-fiber correlations between transcutaneous USVH and histology of the carotid plaque[7] and GSM differences between acute and subacute venous thrombosis.[6] At the moment, we are investigating different types of edema, cellulites, acute or subacute thrombi associated with chronic venous obstruction, and tissue changes after saphenous vein treatment. Additional kidney research will focus on specific data of distinct pathologies imaged by ultrasound as already mentioned in the literature.[13–29] Ultrasound tissue characterization should therefore expand to evaluation of localized regions of the kidney such as cortex, possibly superior, mid, and lower; medulla; central fat; collection system including calyces, infundibula and pelvis; parenchyma, interlobar region; masses; even perirenal tissue; and others, to define specific changes associated with specific disorders. As USTC evolves to USVH, specific brightness intervals may change as kidney tissue is properly identified. In summary, most normal young kidney

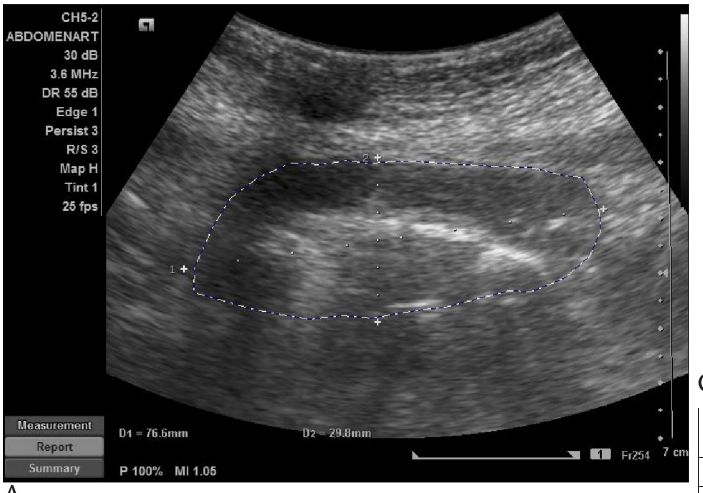

A

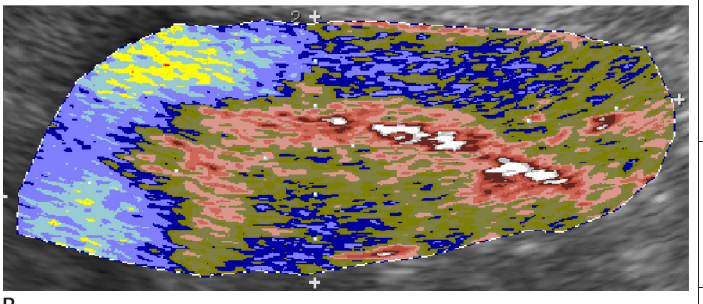

B

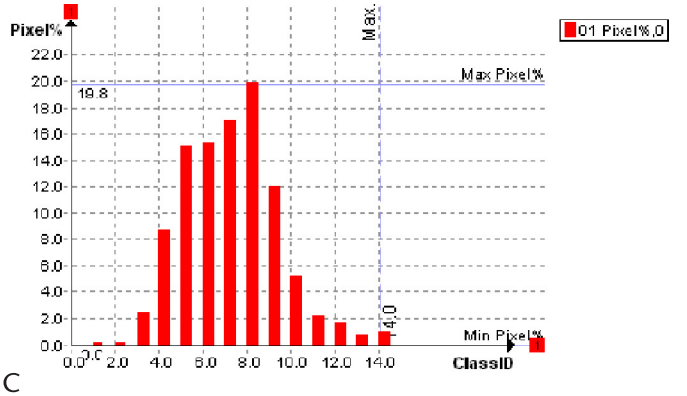

C

Interval Identification (ID)	Gray From	To	Pixel No%	Color
Nonechoic (blood-like)	0	4	0.004	
Hypoechoic I (blood/fat-like)	5	7	0.013	
Hypoechoic II (fat-like)	8	26	2.388	
Hypoechoic III (fat/muscle-like)	27	40	8.603	
Hypoechoic IV (hypoechoic muscle-like)	41	60	14.942	
Echoic I (hyperechoic muscle-like)	61	76	15.210	
Echoic II (hypoechoic muscle/fiber-like)	77	90	16.912	
Echoic III (hyperechoid muscle/fiber-like)	91	111	19.764	
Echoic IV (fiber-like lower level)	112	132	11.916	
Hyperechoic I (fiber-like mid lower lever)	133	153	5.039	
Hyperechoic II (fiber-like midhigher level)	154	174	2.117	
Hyperechoic III (fiber-like mid higher level)	175	196	1.583	
Hyperechoic IV (fiber/calcium-like)	197	210	0.623	
Saturated (white calcium-like)	211	255	0.884	

ID associated with virtual histology of carotid plaques (reference 3); gray scale brightness level from-to based on 256 amplitude levels; percentage of pixels in the interval; color arbitrarily assigned by analyst.

D

FIGURE 2. Example of virtual USTC applied to a transplanted kidney with abnormalities. A, B-mode image from a common ultrasound instrument. B, Colorized image representing various pixel brightness levels. C, Histogram showing pixel brightness distribution. D, Table defining 14 levels of grayscale pixel brightness transformed into artificial colors.

ultrasound echoes were in the "8–60" interval of images with 256 levels of brightness. Pixel brightness was mostly in the hypoechoic relative interval. Kidney GSM was in the 30-to-50 region. An abnormality should be suspected if kidney regions have nonechoic, echoic, or hyperechoic pixels or if the general kidney GSM is below 30 or more than 50. Future research may associate USTC to specific pathologies. Ultrasound virtual histology could become a practical subset of USTC.

REFERENCES

1. Layland J, Wilson AM, Lim I, et al. Virtual histology: a window to the heart of atherosclerosis. *Heart Lung Circ*. 2011;20:615–621.
2. Deftereos S, Giannopoulos G, Kossyvakis C, et al. Virtual histology. Review Article. *Hellenic J Cardiol*. 2010;51:235–244.
3. Lal BK, Hobson RW 2nd, Pappas PJ, et al. Pixel distribution analysis of B-mode ultrasound scan images predicts histologic features of atherosclerotic carotid plaques. *J Vasc Surg*. 2002;35:1210–1217.
4. Biasi G, Froio A, Diethrich EB, et al. Carotid plaque echolucency increases the risk of stroke in carotid stenting. *Circulation*. 2004;110:756–762.
5. Marks NA, Ascher E, Hingorani AP, et al. Gray-scale median of the atherosclerotic plaque can predict success of lumen re-entry during subintimal femoral-popliteal angioplasty. *J Vasc Surg*. 2008;47:109–116.
6. Cassou-Birckholz MF, Engelhorn CA, Salles-Cunha SX, et al. Assessment of deep venous thrombosis by grayscale median analysis of ultrasound images. *Ultrasound Q*. 2011;27:55–61.
7. Menezes FH, Silveira TC, Silveira SAF, et al. Virtual histology of carotid atheroma based in B-mode ultrasound. Preliminary results of in vivo ultrasound vs endarterectomy plaque histology. Presented at the Biannual Conference of the Brazilian Society of Angiology and Vascular Surgery, Sao Paulo, SP, October 10–15, 2011.
8. Menezes FH, Silveira SAF, Salles-Cunha SX. Pixel characterization for development of ultrasound-based virtual histology of deep venous thrombosis. Presented at the 34th SVU Annual Conference, Chicago, IL, June 16–18, 2011. E-published at www.svunet.org (members only) Presentation Abstract 109, p.3.
9. Salles-Cunha SX. Ultrasound virtual histology applied in the differentiation of lymphedema. Presented at the I Jornada Internacional de Plebologia e Linfologia Santista, Santos, SP, August 11–13, 2011.
10. Engelhorn ALDV, Engelhorn CA, Salles-Cunha SX. Initial evaluation of virtual histology ultrasonographic techniques applied to a case of renal transplant. Poster presented at the 34th SVU Annual Conference, Chicago, IL, June 16–18, 2011. E-published at www.svunet.org (members only) Poster Abstract 412, p.20.
11. Engelhorn CA, Engelhorn ALV. Study of transplanted kidney and pancreas. In: Engelhorn CA, de Morais Filho D, Barros FS, et al, eds. *Vascular Ultrasonography: Practical Guide*. 2nd ed. Rio de Janeiro, Brazil: Di Livros Editora LTDA; 2011:197–212.
12. Salles-Cunha SX, Silveira AFS, Menezes FH. Ultrasound virtual histology to grade treatment of lower extremity lymphedema. Poster

presented at the 35th SVU Annual Conference, National Harbor, MD, June 7–9, 2012.
13. Shafuddin A. Imaging evaluation of kidney transplant recipients. *Semin Nephrol*. 2011;31:259–271.
14. Sutherland T, Temple F, Chang S, et al. Sonographic evaluation of renal transplant complications. *J Med Imaging Radiat Oncol*. 2010;54:211–218.
15. Sanchez K, Barr RG. Contrast-enhanced ultrasound detection and treatment guidance in a renal transplant patient with renal cell carcinoma. *Ultrasound Q*. 2009;25:171–173.
16. Jimenez C, Lopez MO, Gonzalez E, et al. Ultrasonography in kidney transplantation: values and new developments. *Transplant Rev (Orlando)*. 2009;23:209–213.
17. Irshad A, Acherman SJ, Campbell AS, et al. An overview of renal transplantation: current practice and use of ultrasound. *Semin Ultrasound CT MR*. 2009;30:298–314.
18. Jung JW, Kirby CL. Quality assurance case of the day: normal hypoechoic perirenal fat mistaken as the renal parenchyma in a patient with small echogenic native kidneys. *Ultrasound Q*. 2008;24:101–103.
19. Cosgrove DO, Chan KE. Renal transplants: what ultrasound can and cannot do. *Ultrasound Q*. 2008;24:77–87.
20. Lockhart ME, Robbin ML. Renal vascular imaging: ultrasound and other modalities. *Ultrasound Q*. 2007;23:279–292.
21. Heller MT, Tublin ME. Detection and characterization of renal masses by ultrasound: a practical guide. *Ultrasound Q*. 2007;23:269–278.
22. Park SB, Kim JK, Cho KS. Complications of renal transplantation: ultrasonographic evaluation. *Ultrasound Med*. 2007;26:615–633.
23. Maizlin ZV, Vos PM, Cooperberg PL. Is it a fibroid? Are you sure? Sonography with MRI assistance. *Ultrasound Q*. 2007;23:55–62.
24. Correas JM, Claudon M, Tranquart F, et al. The kidney: imaging with microbubble contrast agents. *Ultrasound Q*. 2006;22:53–66.
25. Wilson SR, Burns PN. Microbubble contrast for radiological imaging: 2. Applications. *Ultrasound Q*. 2006;22:15–18.
26. Khaati NJ, Hill MC, Kimmel PL. The role of ultrasound in renal insufficiency: the essentials. *Ultrasound Q*. 2005;21:227–244.
27. Friedewald SM, Molmenti EP, Friedewald JJ, et al. Vascular and nonvascular complications of renal transplants: sonographic evaluation and correlation with other imaging modalities, surgery and pathology. *J Clin Ultrasound*. 2005;33:127–139.
28. Baxter GM. Imaging in renal transplantation. *Ultrasound Q*. 2003; 19:123–138.
29. Choyke PL, Daryanani K. Intraoperative ultrasound of the kidney. *Ultrasound Q*. 2001;17:245–253.

